atmosphere

MDPI

Article

Spatiotemporal Characteristics and Statistical Model Prediction of Potential Evaporation during the Growing Season in Ningxia

Zhe Liu [1], Quan Sun [1,*], Dejia Xu [1], Wenbo Fan [2], Rui Wang [1] and Peng Jiang [1]

[1] Agricultural College of Ningxia University, Ningxia University, Yinchuan 750021, China
[2] School of Water Conservancy and Construction Engineering, Shihezi University, Shihezi 832000, China
* Correspondence: 103050@stu.nxu.edu.cn

Abstract: Based on the daily data of 24 meteorological warfare points in Ningxia, the potential evaporation (ET0), the Mann–Kendall test (MK), and inverse distance weight interpolation were used to analyze the temporal and spatial changes in the potential evaporation at different scales, and the Pearson correlation coefficient was used to determine the growth rate in Ningxia. The atmospheric circulation influencing factors of seasonal potential evaporation were established, and the prediction model of potential evaporation in the growing season in Ningxia was established by stepwise linear regression, using mean absolute error (MAE), root mean square error (RMSE), and mean absolute percentage error (MAPE). The error test was carried out, and the results show the following: (1) The areas with larger potential evaporation during the growing season are mainly the central area of Ningxia and the northern side of the northern area. The presence on the north side tends to decrease. (2) On the monthly scale, the potential evaporation continued to increase from April to June, reached the maximum in June, continued to decrease from July to October, and was the smallest in October. (3) During the MK test in the growing season, the change in potential evaporation in the growing season showed an "increase–decrease" trend. The results of the monthly MK test show that the potential evaporation in April, May, and June has shown an increasing trend over the past 30 years, and the UF value in July, August, and October has been relatively high. The change trend of potential evaporation has been relatively stable, and the potential evaporation in September has shown a downward trend over the past 20 years. (4) The prediction model of potential evaporation in the growing season established by the circulation factor has shown a good effect in Ningxia and can be used to establish the scheduling prediction of irrigation water.

Keywords: potential evaporation; circulation index; spatiotemporal characteristics; Ningxia

Citation: Liu, Z.; Sun, Q.; Xu, D.; Fan, W.; Wang, R.; Jiang, P. Spatiotemporal Characteristics and Statistical Model Prediction of Potential Evaporation during the Growing Season in Ningxia. *Atmosphere* **2022**, *13*, 1654. https://doi.org/10.3390/atmos13101654

Academic Editor: Hanbo Yang

Received: 12 August 2022
Accepted: 7 October 2022
Published: 11 October 2022

1. Introduction

Potential evapotranspiration refers to the total amount of water that can be evapotranspired into the air under conditions of sufficient moisture. It is usually calculated by the Penman–Monteith (FAO-56) (P-M) formula [1]. Potential evapotranspiration is an important factor in the hydrological cycle and irrigation scheduling [2,3], global climate change has had a great impact on the vapor content of the atmosphere [4], and the potential evaporation has an extremely important impact on irrigation planning, especially for high-frequency irrigation systems and shallow-rooted vegetation [5,6]; therefore, the prediction of potential evaporation is of great significance in agricultural production and the sustainable development of water resources.

There is a significant correlation between the changes in and anomalies of global atmospheric circulation, and a circulation anomaly in one region can cause a circulation anomaly in another region, far away [7]. Teleconnection is the result of long-term natural climate change [8] and has the characteristics of periodicity [9], persistence [10], strong predictability [11], and hysteresis [12] for local climate impacts. Previous studies have shown that atmospheric circulation has a certain influence on wind speed, temperature,

humidity, sunshine hours, etc. [13–16]. These parameters are all important factors in the calculation of potential evaporation, and through teleconnection, the hydrometeorological forecast increases the feasibility of the potential evaporation forecast and plays a guiding role in the hydrological cycle and agricultural production.

The variation in potential evapotranspiration (ET0) in China has significant temporal and spatial differences. Predicting potential evapotranspiration is particularly important for arid and semi-arid regions [17–19]. Ningxia Hui Autonomous Region is located in arid and semi-arid regions of China. We used meteorological stations to explore the temporal and spatial variability of potential evaporation in Ningxia, and used the circulation index to establish a forecasting model for the growing season in Ningxia.

2. Study Area, Dataset and Methods

2.1. Study Area

Ningxia is located in the Yellow River system, which belongs to the temperate continental arid and semi-arid climate, with low annual precipitation, a high degree of evaporation, and frequent droughts. Between 35°14′−39°23′ N latitude and 104°17′′−107°39′ E longitude, as shown in Figure 1, the terrain is high in the south and low in the north. It is divided into three major areas from north to south: the northern irrigation area (Shitanjing, Huinong, Shizuishan, Pingluo, Taole, Helan, Yinchuan, Qingtongxia, Lingwu, Wuzhong, Zhongning, and Zhongwei), the central drought belt (Yanchi, Mahuang Mountain, Weizhou, Tongxin, Haiyuan, and Xingrenbao), and the southern mountainous area (Xiji, Guyuan, Liupanshan, Longde, and Jingyuan).

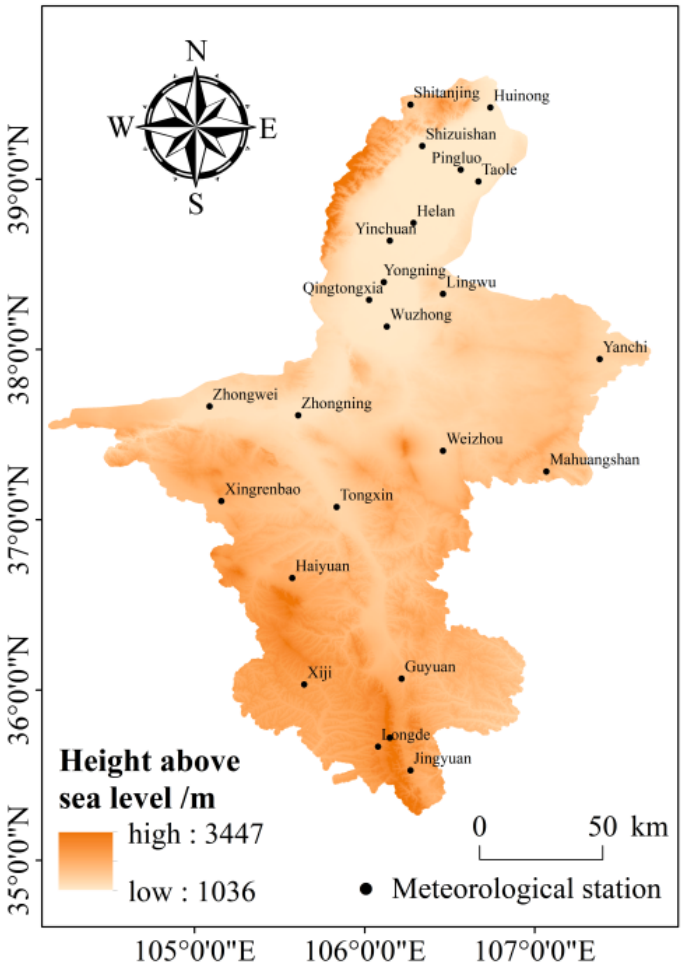

Figure 1. Altitude and distribution of meteorological stations in Ningxia.

2.2. Meteorological Data Sources

Ningxia meteorological data were selected from the National Meteorological Center of the China Meteorological Administration. In order to ensure the uniformity of data time, daily meteorological data from 1982 to 2020 were used, and five meteorological factors from 24 meteorological stations in Ningxia were selected, namely maximum temperature, minimum temperature, wind speed, sunshine hours, and relative humidity, alongside atmospheric circulation data from 1981 to 2020. The 130 circulation indices were divided into monthly data. The data came from the China Meteorological Administration, including 88 atmospheric circulation indices, 26 SST indices, and 16 other indices.

2.3. Research Methods

2.3.1. Penman–Monteith Equation (ET0)

ET_0 is the possible evapotranspiration of crops, which can be calculated by the Penman–Monteith formula recommended by the Food and Agriculture Organization of the United Nations (FAO, 1998).

$$ET_0 = \frac{0.408\Delta(R_n - G) + \gamma\frac{900}{T+273}U_2(e_s - e_a)}{\Delta + \gamma(1 + 0.34U_2)} \quad (1)$$

where the unit of $ET0$ is mmd. Δ is the slope value of the relationship between saturated water vapor pressure and temperature (kPa/°C); R_n represents the net radiation from the ground (MJ/m^2); G represents the soil heat flux (MJ/(m^2·d)), which is so small as to be negligible; γ represents the hygrometer constant (kPa/°C); T represents the daily average temperature (°C); U_2 represents the wind speed at a height of 2 m (m/s); e_s represents the saturated vapor pressure (kPa); and e_a represents the actual water vapor pressure (kPa/°C).

2.3.2. Pearson Correlation Analysis

If two sets of data, X: (X_1, X_2, … , X_n) and Y: (Y_1, Y_2, … , Y_n), are population data, then we obtain the following

$$Cov(X, Y) = \frac{\sum_{i=1}^{n} \frac{(X_i - E(X))}{\sigma_x} \frac{(Y_i - E(Y))}{\sigma_y}}{n} \quad (2)$$

where n is the total sample size. σ_x, σ_y are the standard deviations of X and Y, respectively. Correlation analysis is used to measure the deviation of each dimension from its mean and the overall error of the two variables. If it is positive, it is positively correlated, and if it is negative, it is negatively correlated. The Pearson correlation coefficient was used to determine the lag relationship between the circulation index and the potential evaporation index during the growing season in Ningxia.

2.3.3. Variance Inflation Factor (VIF)

Multicollinearity in stepwise regression models is a condition that occurs when some predictors in the model are correlated with other predictors. Multicollinearity can be a serious problem as it can cause the variance of regression coefficients to increase, making them unstable.

$$VIF = \frac{1}{1 - R_i^2} \quad (3)$$

where R_i is the negative correlation coefficient of the independent variable x_i in the regression analysis of the remaining independent variables. The larger the variance inflation coefficient VIF, the greater the possibility of collinearity between independent variables. In general, if the variance inflation factor exceeds 10, the regression model has severe multicollinearity.

2.3.4. Mean Absolute Error (MAE)

The mean absolute error is the average of the absolute errors and can better reflect the actual situation of the predicted value error.

$$MAE = \frac{1}{N}\sum_{i=1}^{N}|f_i - y_i| \tag{4}$$

where f_i is the predicted value, y_i is the actual value, and N is the number of data series.

2.3.5. Root Mean Square Error (RMSE)

The root mean square error is the square root of the ratio of the square of the predicted value's deviation from the true value to the number of observations, n. It measures the deviation between the predicted value and the true value and is sensitive to outliers in the data.

$$RMSE = \sqrt{\frac{1}{N}\sum_{t=1}^{N}(f_t - y_t)^2} \tag{5}$$

where f_t is the actual value, y_t is the predicted value, and N is the number of data series.

2.3.6. Mean Absolute Percentage Error (MAPE)

The smaller the value of *MAPE*, the better the accuracy of the prediction model.

$$MAPE = \frac{100\%}{n}\sum_{i=1}^{n}\left|\frac{y_i' - y_i}{y_i}\right| \tag{6}$$

where y_i is the actual value, $y_i^{'}$ is the predicted value, and n is the number of sample sequences.

2.3.7. Mann–Kendall Trend Test

The Mann–Kendall trend test is a method recommended by the World Meteorological Organization for time series analysis. Given a significance level, if the significance is at 0.05, then the critical value is ±1.96; plot UF_k and UB_k graphs and ±1.96 two straight lines again on a graph, if the *UF* value is greater than 0, then the series shows an upward trend, less than 0 indicates a downward trend When they exceed the critical line, it indicates a significant upward or downward trend. If the UF_k and UB_k curves intersect and the intersection point is within the critical line, then the moment corresponding to the intersection point is the time when the mutation starts.

For a time series $X_1, X_2, \ldots, X_n$ with n sample sizes, construct an order column.

$$S_k = \sum_{j=1}^{k} r_j,\ r_j = \begin{cases} 1(X_j > X_i) \\ 0(X_j \le X_i) \end{cases},\ i = 1, 2, 3, \ldots\ldots j;\ k = 1, 2, 3, \ldots\ldots n \tag{7}$$

where r_j denotes the cumulative number of X_i greater than X_j ($1 \le j \le i$), S_k is the statistic, and i and j denote the number of sequences.

$$UF_k = \frac{(S_k - E[S_k])}{\sqrt{Var[S_k]}} \tag{8}$$

where UF_k = 0 when k = 1. $E[S_k]$, $Var[S_k]$ are the mean and variance of the cumulative number S_k, respectively, which can be calculated when $X_1, X_2, \ldots, X_n$ are independent of each other and have the same continuous distribution by the following equation.

$$E[S_k] = \frac{k(k-1)}{4},\ Var[S_k] = \frac{k(k-1)(2k+5)}{72},\ 1 \le k \le n \tag{9}$$

where $E(S_k)$ is the mean of the cumulative number S_k, $Var(S_k)$ is the cumulative number S_k variance, and k is the number of current series.

$$UB_k = -UF_k \tag{10}$$

where $UB_k = 0$. UB_k is not simply equal to the negative value of UF_k, but is inverted and then taken as negative, where UF_k is calculated from the inverse sequence. The intersection of UF and UB is the mutation point.

3. Results and Analysis

3.1. Distribution and Trend of Potential Evaporation

3.1.1. Distribution and Trend of Potential Evaporation in the Growing Season

The spatial characteristics of potential evaporation in the growing season of Ningxia Autonomous Region are shown in Figure 2. The potential evaporation in Ningxia is between 585.03 mm and 1146.23 mm, with the potential evaporation in the middle of the central arid zone and in the north side of the northern region being larger, between 1000.34 and 1146.23 mm, and the potential evaporation in the southern region smaller, between 585.03 and 781.65 mm. The west side of the central region of Ningxia Hui Autonomous Region demonstrates a greater increasing trend, and its value is between 13.91 and 41.51. There is a decreasing trend in the east and north sides of Ningxia Hui Autonomous Region, and the decreasing trend is between −30.72 and 0.00 mm.

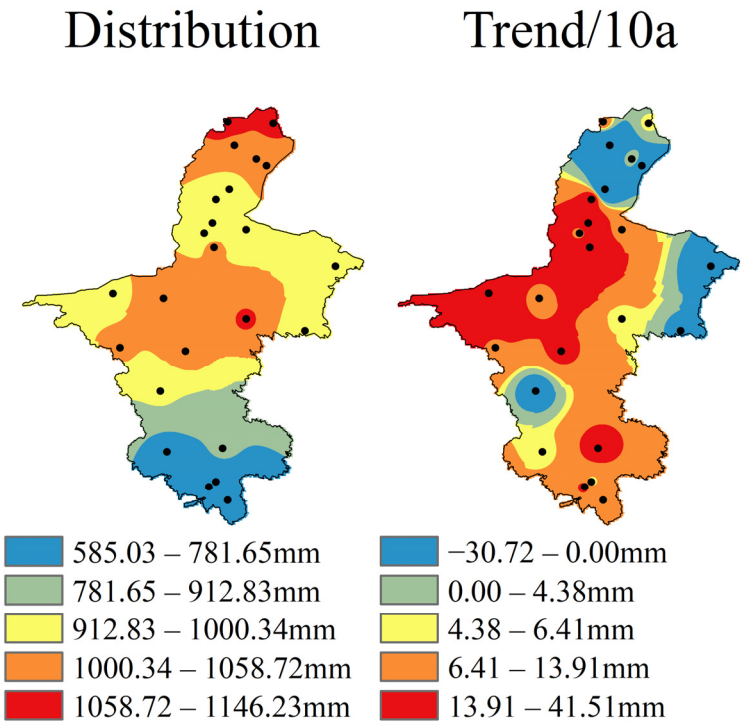

Figure 2. Spatial characteristics of potential evaporation during the growing season in Ningxia Autonomous Region.

3.1.2. Monthly Potential Evaporation Distribution and Trend in the Growing Season

The monthly spatial characteristics of the potential evaporation in the growing season of Ningxia Autonomous Region are shown in Figure 3. The distribution of the potential evaporation in each month is exemplified by the potential evaporation in the central region and the northern region being larger, and the potential evaporation in the southern region being smaller. The potential evaporation continued to increase in June, and reached its largest value in June, with a value between 103.32 and 209.32 mm. The potential evaporation continued to decrease from July to October, and the potential evaporation in October was

the smallest, with a value between 52.57 and 86.65 mm. The increasing trend of potential evaporation from April to June is relatively obvious, and the areas with a greater increasing trend are mainly concentrated in the west of the central region. The north of the northern region and the east of the central region have a decreasing trend. From July to October, the potential evaporation has a decreasing trend. The decreasing trend in September is the most obvious, but most areas show a decreasing trend to some extent. The northern part of the northern region and the eastern part of the central region have the largest decreasing trend, and the value is between −7.58 and −3.54.

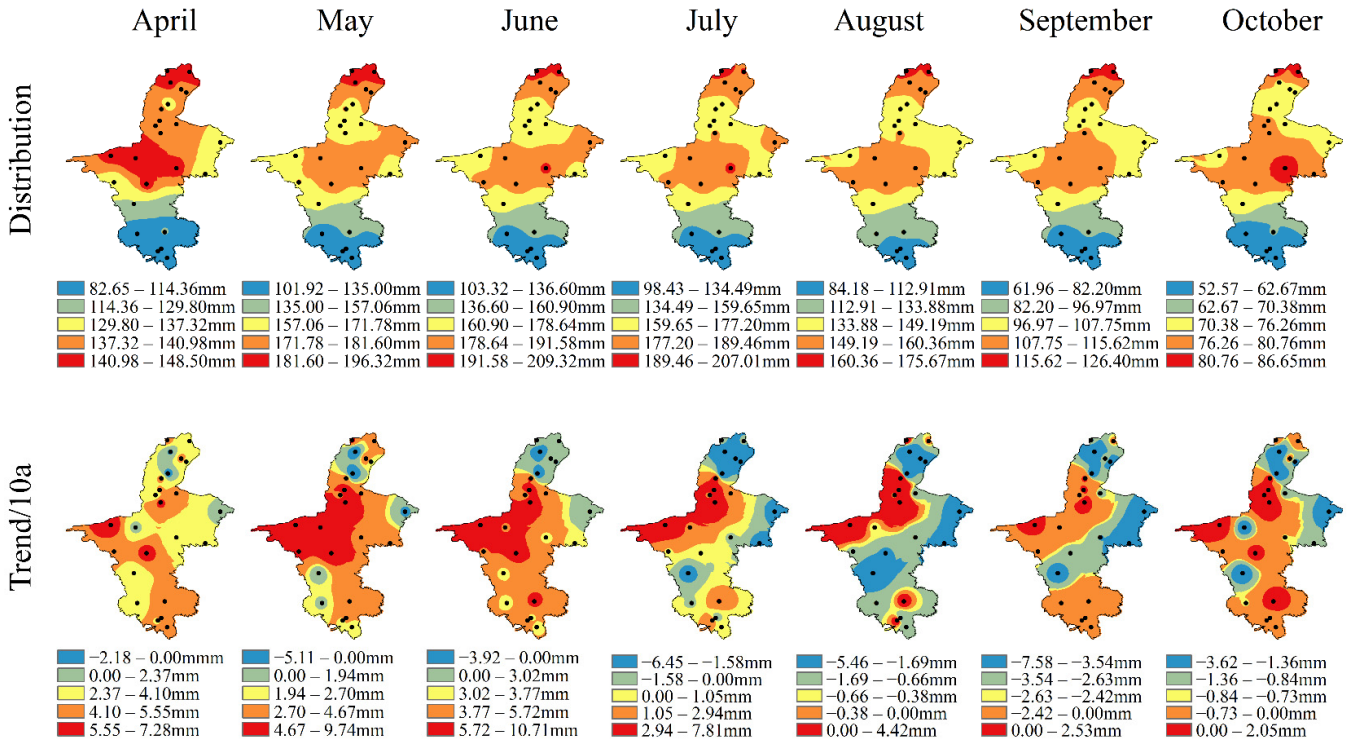

Figure 3. Spatial characteristics of monthly potential evaporation during the growing season in Ningxia Autonomous Region.

3.1.3. Time Evolution Trend and Mutation of Potential Evaporation

The temporal change law of potential evaporation (ET0) in Ningxia Hui Autonomous Region is shown in Figure 4. The UF value shows an "increase–decrease" trend on the time scale of the growing season. There is a downward trend in 2020, but the UF value greater than 0 indicates that the potential evaporation in the growing season is still rising, although the rising trend is decreasing. The mutation point appeared in 1988. From April to June, 1992–2020, the UF value showed an increasing trend. During this period, the potential evaporation increased. The mutation points appeared in 1998, 1993, and 1990, and appeared more frequently in July and August during the period from 1982 to 2020. At the mutation point, the change in UF value is relatively stable, and the increase in potential evaporation is not obvious. In September, the potential evaporation showed a downward trend from 1998 to 2020, and the mutation point appeared in 2005. The mutation point in October appeared in 1986, and the UF value changed. According to the results of the MK test, the potential evaporation in April, May, and June showed an increasing trend over the past 30 years, the UF value and potential evaporation in July, August, and October were relatively stable, and the potential evaporation in September showed a decline over the past 20 years.

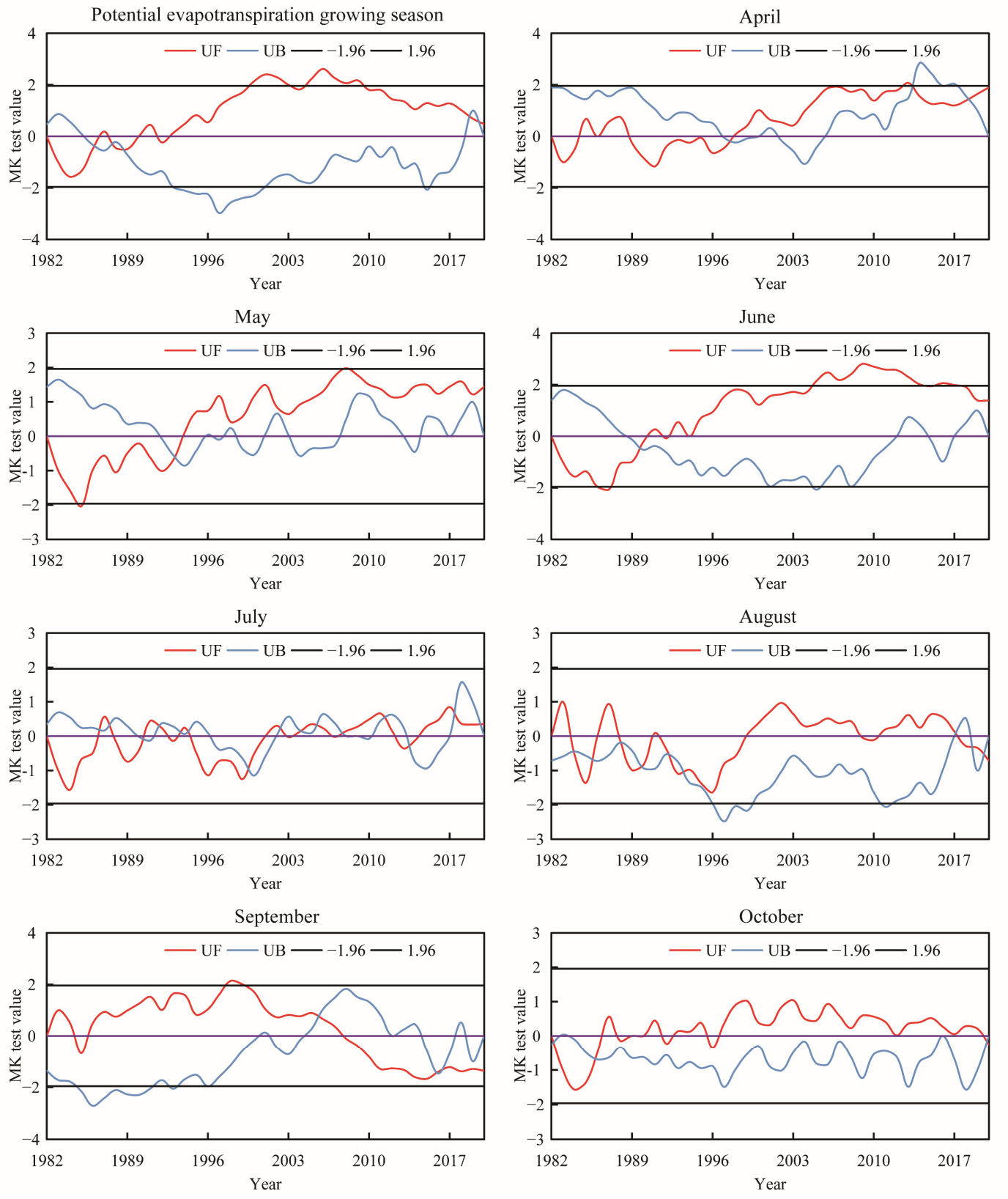

Figure 4. Monthly MK test values of potential evaporation during the growing season.

3.2. Prediction of Potential Evaporation

3.2.1. Factor Screening and Model Construction

Pearson correlation analysis was carried out to assess the potential evaporation in the growing season and the circulation index combined in different time periods (shown in Table 1). Because the growing season is from April to October, the forecast factor was selected from April of the previous year. Using the circulation factor from March of that year, 1560 correlation coefficients were actually obtained. On this basis, factor screening was carried out. The correlation analysis between the atmospheric circulation index at different time periods and the potential evaporation in the growing season was carried out. After screening, 33 correlation coefficients were finally obtained at the 0.05 significance level. Atmospheric circulation factors and time periods were tested, of which nine circulation indices met the 0.01 significance level.

3.2.2. Establishment and Verification of the Potential Evaporation Prediction Model in the Growing Season

Based on the atmospheric circulation index factors in Table 1, the stepwise regression model was used to build the model. The model with a variance inflation factor (VIF) less than 5 was selected. Table 2 shows, The variance inflation factor of all models was within 2. The selected atmospheric circulation index factors were from April of the previous year to March of the current year.

3.2.3. Fitting Back-Generation of Potential Evaporation in the Growing Season

The potential evaporation during the growing season in Ningxia is between 585.16 and 1142.81 mm. As shown in Figure 5, the maximum actual value of potential evaporation (1055.85 to 1142.81 mm) is mainly distributed in the north of the northern part of Ningxia and the center of the central Ningxia arid zone. The potential evaporation in the growing season is between 585.14 and 1154.87 mm, and the predicted maximum potential evaporation is between 1062.75 and 1154.87 mm. The predicted potential evaporation distribution is basically consistent with the actual potential evaporation distribution. As shown in the error analysis in Figure 6, the mean absolute error (MAE) is between 13.39 and 35.25, the root mean square error (RMSE) is between 16.33 and 45.18, and the mean absolute percentage error (MAPE) is between 1.83% and 3.52%.

Table 1. Correlation analysis was carried out for potential evaporation in the growing season (April–October) with a time lag of 12 months (April–December of the previous year and January–March of the current year), and a significant p was selected. Atmospheric circulation factor < 0.05.

Time	Numbering	Index Name	Correlation	Time	Numbering	Index Name	Correlation
April of the previous year	X1	Northern Hemisphere Polar Vortex Central Intensity Index	0.338 *	September of the previous year	X19	Western Pacific Subtropical High Northern Boundary Position Index	−0.345 *
April of the previous year	X2	Western North Pacific Typhoon number	0.348 *	September of the previous year	X20	Asian Zonal Circulation Index	0.318 *
May of the previous year	X3	Eastern Pacific Subtropical High Northern Boundary Position Index	−0.394 *	September of the previous year	X21	North Atlantic Triple index	−0.340 *
May of the previous year	X4	Asia Polar Vortex Area Index	−0.440 **	October of the previous year	X22	Western North Pacific Typhoon number	−0.319 *
May of the previous year	X5	Northern Hemisphere Polar Vortex Central Longitude Index	−0.318 *	November of the previous year	X23	Indian Subtropical High Ridge Position Index	0.327 *
May of the previous year	X6	Central Pacific 850 mb Trade Wind Index	0.322 *	November of the previous year	X24	Northern Hemisphere Polar Vortex Area Index	−0.318 *
June of the previous year	X7	North African–North Atlantic–North American Subtropical High Ridge Position Index	0.525 **	November of the previous year	X25	East Atlantic–West Russia Pattern, EA/WR	−0.393 *
June of the previous year	X8	North American Subtropical High Northern Boundary Position Index	0.343 *	December of the previous year	X26	Atlantic Subtropical High Ridge Position Index	0.419 **
June of the previous year	X9	Western Pacific Subtropical High Western Ridge Point Index	0.318 *	January of that year	X27	Western Pacific Subtropical High Ridge Position Index	−0.411 **
June of the previous year	X10	Western Pacific Warm Pool Area Index	0.323 *	January of that year	X28	Pacific Subtropical High Ridge Position Index	−0.332 *
July of the previous year	X11	Asia Polar Vortex Area Index	−0.421 **	February of that year	X29	Asian Zonal Circulation Index	0.332 *
July of the previous year	X12	Northern Hemisphere Polar Vortex Central Latitude Index	0.418 **	February of that year	X30	South Indian Ocean Dipole Index	0.536 **
July of the previous year	X13	East Asian Trough Intensity Index	0.379 *	March of that year	X31	East Asian Trough Position Index	−0.362 *
August of the previous year	X14	North American Subtropical High Ridge Position Index	−0.491 **	March of that year	X32	Polar–Eurasia Pattern, POL	−0.320 *
August of the previous year	X15	Western Pacific Subtropical High Western Ridge Point Index	−0.389 *	March of that year	X33	South Indian Ocean Dipole Index	0.474 **
August of the previous year	X16	Northern Hemisphere Polar Vortex Central Longitude Index	−0.319 *				
Last august	X17	East Pacific 850 mb Trade Wind Index	−0.404 *				
Last august	X18	Oyashio Current SST Index	0.342 *				

* The correlation is significant at the 0.05 level, ** the correlation is significant at the 0.01 level.

Table 2. Models built based on the atmospheric circulation index. Stepwise regression was used to select a suitable model through the expansion factor test (VIF < 10).

City	Model Formulas	Variance Inflation Factor					
Huinong	$y = 1438.701 + 6.856 \times 7 + 0.64 \times 9 - 8.158 \times 11 - 15.609 \times 14$	X7	X9	X11	X14		
		1.263	1.13	1.038	1.091		
Shizuishan	$y = 1675.5 - 0.03 \times 3 - 13.094 \times 10 - 21.89 \times 27 + 51.134 \times 30$	X3	X10	X27	X30		
		1.042	1.118	1.059	1.088		
Yinchuan	$y = 672.282 + 0.224 \times 1 + 6.772 \times 10 - 18.617 \times 14 - 5.996 \times 24 + 0.039 \times 26 + 17.952 \times 33$	X1	X10	X14	X24	X26	X33
		1.32	1.473	1.126	1.239	1.289	1.196
Shitanjing	$y = -1377.114 + 0.114 \times 13 - 23.61 \times 14 + 33.532 \times 33$	X13	X14	X33			
		1.314	1.045	1.295			
Pingluo	$y = 311.32 + 0.228 \times 1 - 17.432 \times 14 + 5.104 \times 29 + 23.766 \times 30$	X1	X14	X29	X30		
		1.071	1.034	1.122	1.179		
Taole	$y = 1497.921 - 0.029 \times 3 - 21.713 \times 4 - 8.443 \times 11 + 28.622 \times 30$	X3	X4	X11	X30		
		1.048	1.037	1.192	1.17		
Helan	$y = 1969.009 - 0.049 \times 03 - 42.471 \times 04 - 3.861 \times 12 - 0.084 \times 19 + 43.525 \times 30$	X3	X4	X12	X19	X30	
		1.046	1.245	1.639	1.109	1.245	
Yongning	$y = 1544.971 - 13.188 \times 14 - 0.176 \times 16 - 16 \times 17 + 10.35 \times 18 + 0.038 \times 26 + 22.343 \times 33$	X14	X16	X17	X18	X26	X33
		1.163	1.2	1.306	1.309	1.277	1.262
Lingwu	$y = 621.255 + 0.175 \times 1 + 0.447 \times 9 - 17.038 \times 14 - 9.442 \times 17 + 19.333 \times 33$	X1	X9	X14	X17	X33	
		1.151	1.089	1.092	1.182	1.097	
Qingtongxia	$y = 1292.535 - 25.765 \times 28 + 9.383 \times 29 - 73.376 \times 32$	X28	X29	X32			
		1.026	1.04	1.033			
Wuzhong	$y = 1407.758 - 36.337 \times 4 + 16.279 \times 10 - 34.602 \times 17 + 9.421 \times 20$	X4	X10	X17	X20		
		1.01	1.168	1.068	1.095		
Zhongning	$y = 1498.873 + 0.673 \times 09 - 11.268 \times 14 - 11.659 \times 28 + 45.472 \times 30 - 32.359 \times 32$	X9	X14	X28	X30	X32	
		1.044	1.13	1.122	1.01	1.035	
Zhongwei	$y = 1935.119 + 4.937 \times 8 + 8.996 \times 10 - 18.349 \times 17 - 6.358 \times 24 - 18.253 \times 27 - 2.936 \times 31$	X8	X10	X17	X24	X27	X31
		1.154	1.383	1.177	1.262	1.165	1.351
Tongxin	$y = 2019.003 - 16.043 \times 14 - 0.614 \times 15 - 0.185 \times 16 - 5.315 \times 24 + 22.342 \times 33$	X14	X15	X16	X24	X33	
		1.156	1.177	1.164	1.153	1.201	
Xiji	$y = 789.801 + 17.915 \times 2 - 0.038 \times 3 - 0.072 \times 19 - 20.455 \times 21 - 0.659 \times 31 + 13.386 \times 33$	X02	X03	X19	X21	X31	X33
		1.094	1.171	1.196	1.465	1.165	1.167
Haiyuan	$y = 947.905 + 29.972 \times 2 - 0.035 \times 3 - 0.376 \times 15 + 23.52 \times 33$	X2	X3	X15	X33		
		1.074	1.075	1.223	1.198		

Table 2. *Cont.*

City	Model Formulas	Variance Inflation Factor					
Yanchi	$y = 1398.19 - 0.03 \times 3 - 21.875 \times 4 - 0.435 \times 15 - 0.044 \times 19 + 43.928 \times 25 + 39.461 \times 30$	X3	X4	X15	X19	X25	X30
		1.039	1.138	1.464	1.206	1.55	1.559
Mahuangshan	$y = 1067.008 + 34.322 \times 2 + 0.933 \times 9 + 4.036 \times 12 - 16.849 \times 27 + 44.168 \times 30 - 2.102 \times 31$	X2	X9	X12	X27	X30	X31
		1.08	1.089	1.24	1.053	1.28	1.11
Xingrenbao	$y = 2114.237 - 8.852 \times 11 - 17.166 \times 14 - 6.311 \times 24 + 0.058 \times 26 + 23.573 \times 33$	X11	X14	X24	X26	X33	
		1.248	1.095	1.132	1.114	1.199	
Weizhou	$y = 435.339 + 0.237 \times 1 + 0.672 \times 9 - 21.703 \times 14 + 31.121 \times 33$	X1	X9	X14	X33		
		1.1	1.012	1.032	1.085		
Guyuan	$y = -1877.545 - 0.047 \times 3 + 0.112 \times 13 - 0.197 \times 15 - 0.073 \times 19 - 24.972 \times 21 - 6.885 \times 24$	X03	X13	X15	X19	X21	X24
		1.066	1.468	1.24	1.351	1.827	1.145
Liupanshan	$y = 945.127 + 12.909 \times 2 - 14.132 \times 14 - 0.062 \times 19 + 4.85 \times 29 - 29.462 \times 30 + 34.969 \times 33$	X2	X14	X19	X29	X30	X33
		1.192	1.226	1.13	1.146	4.617	4.283
Longde	$y = 1004.488 - 0.031 \times 3 - 14.066 \times 4 - 9.009 \times 17 - 0.078 \times 19 - 18.702 \times 21 + 17.085 \times 30$	X3	X4	X17	X19	X21	X30
		1.259	1.106	1.337	1.239	1.741	1.237
Jingyuan	$y = 1040.664 + 20.605 \times 2 - 10.903 \times 14 - 0.089 \times 19 + 0.05 \times 26 + 27.748 \times 33$	X2	X14	X19	X26	X33	
		1.149	1.1	1.036	1.038	1.042	

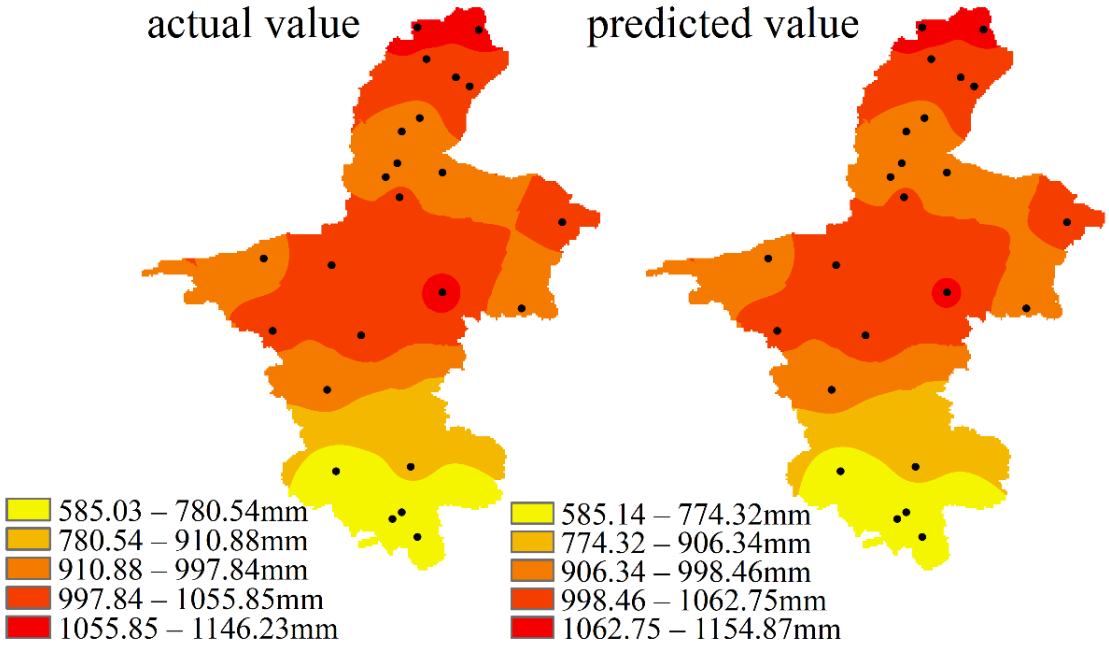

Figure 5. The annual average distribution of the actual and predicted values of the fitted back-alternative.

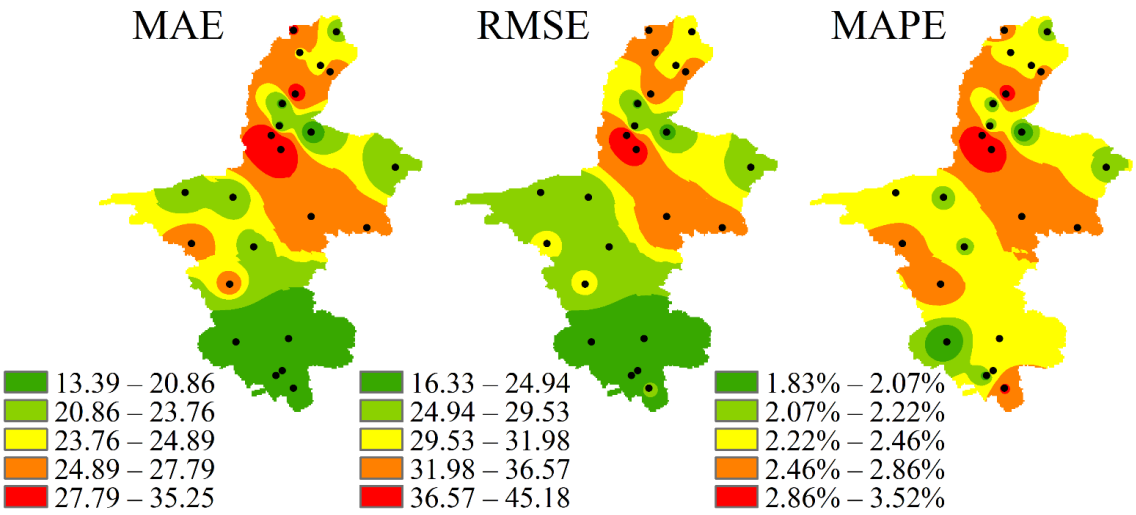

Figure 6. Fitting back-substitution error analysis (mean absolute error (MAE), root mean square error (RMSE), and mean absolute percentage error (MAPE)).

3.2.4. Extrapolated Forecast of Potential Evaporation during the Growing Season

Figure 7 shows the distribution of the extrapolated forecast and the actual value, as well as the difference between the two. By comparing the distribution of the actual value and the predicted value from 2016 to 2020, although the potential evaporation has space and time differences, the predicted result is basically consistent with the actual value of the potential evaporation. The difference between the actual value and the predicted value in Ningxia is between −57.32 and 136.98. Through the error analysis of the extrapolated predictions in Figure 8, the mean absolute error (MAE) is between 19.47 and 70.11. The distribution of root mean square error (RMSE) and mean absolute error (MAE) is roughly consistent, and the root mean square error (RMSE) in Ningxia is between 24.66 and 81.78. The mean absolute percentage error (MAPE) of all regions is within 10%, among which

the northern region (green region) has the smallest error, between 2.12 and 3.97%, and the southern region has a larger prediction error.

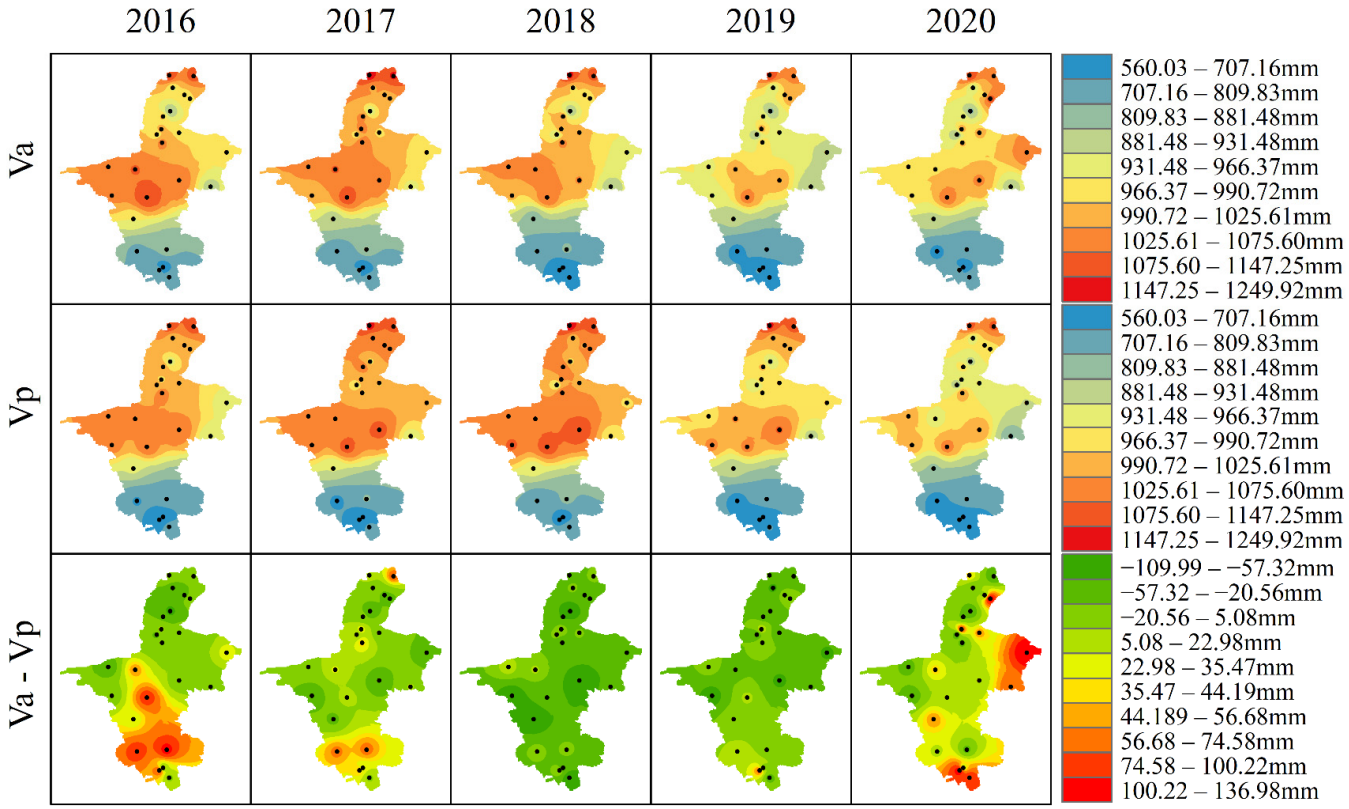

Figure 7. Distribution of and differences between actual and predicted values, unit/mm (Va is the actual value from 2016 to 2020, Vp is the predicted value from 2016 to 2020, and Va-Vp is the actual value minus the predicted value).

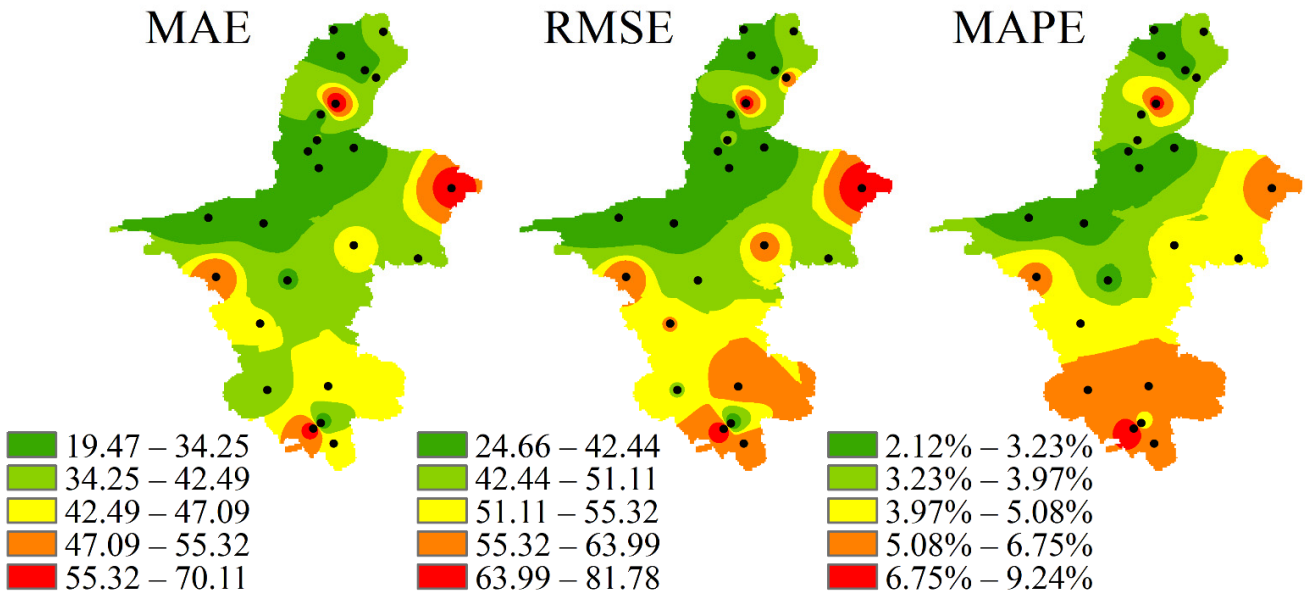

Figure 8. Analysis of extrapolated forecast error, mean absolute error (MAE), root mean square error (RMSE), and mean absolute percentage error (MAPE).

3.2.5. Monthly Fitting Back-Generation of Potential Evaporation in the Growing Season

Based on the circulation factor, a monthly potential evaporation prediction model is established, and the model is established by using a circulation factor that is pushed 12 months ahead of the predicted month. The modeling steps are consistent with the potential evaporation in the growing season, and collinearity (VIF) less than 5 is selected. The basic information of the selected model is shown in Tables 3 and 4. Models, due to space reasons, are no longer listed one by one. According to Figure 9, the fitted values from 1982 to 2015 are basically consistent with the actual values. As shown in Figure 10, the mean absolute error (MAE) is generally between 1.50 and 12.00 in each month, and the red area is larger in May, June, and July, indicating that the mean absolute error (MAE) error is larger; the blue areas are larger in August, September, and October, indicating a smaller mean absolute error (MAE). The root mean square error (RMSE) is generally between 1.50 and 14.00 in each month, and the red area is larger in May, June, and July, indicating that the root mean square error (RMSE) is larger. On the other hand, the blue area in August, September, and October is larger, and the root mean square error (RMSE) is small. The mean absolute percentage error (MAPE) is between 1.00% and 12.00% across all months as a whole. In October, the red area is larger, indicating that the mean absolute percentage error (MAPE) is larger; in August, the blue area is larger, indicating that the mean absolute percentage error (MAPE) is smaller.

Table 3. Number of selected circulation index factors (correlation significant $p < 0.05$).

April	May	June	July	August	September	October
127	138	70	36	62	100	88

Table 4. Stepwise asymptotic regression to select the number of factors (VIF < 10).

Place	April	May	June	July	August	September	October
Huinong	5	5	5	4	14	5	7
Shitanjing	6	5	6	3	6	6	5
Shizuishan	5	5	3	10	5	9	7
Pingluo	7	9	5	4	5	7	5
Taole	6	4	7	6	12	5	5
Helan	4	5	3	5	7	5	8
Yinchuan	6	7	12	3	9	5	4
Yongning	6	6	5	6	16	10	7
Lingwu	6	5	4	6	6	5	6
Qingtongxia	6	8	5	9	8	4	5
Wuzhong	4	5	9	4	4	13	7
Zhongning	8	8	5	5	5	9	6
Zhongwei	3	5	6	8	4	14	10
Tongxin	9	4	14	6	13	5	7
Haiyuan	5	6	13	3	5	5	10
Yanchi	4	5	5	5	10	5	5
Mahuangshan	5	6	7	6	4	9	5
Xingrenbao	7	3	6	4	4	5	5
Weizhou	5	5	4	5	7	8	6
Xiji	5	9	5	3	4	2	7
Guyuan	6	5	4	9	5	4	5
Liupanshan	5	8	5	3	8	4	4
Longde	8	11	9	5	5	5	5
Jingyuan	6	4	5	3	8	3	7

Figure 9. The Ningxia area fitted with back-generation.

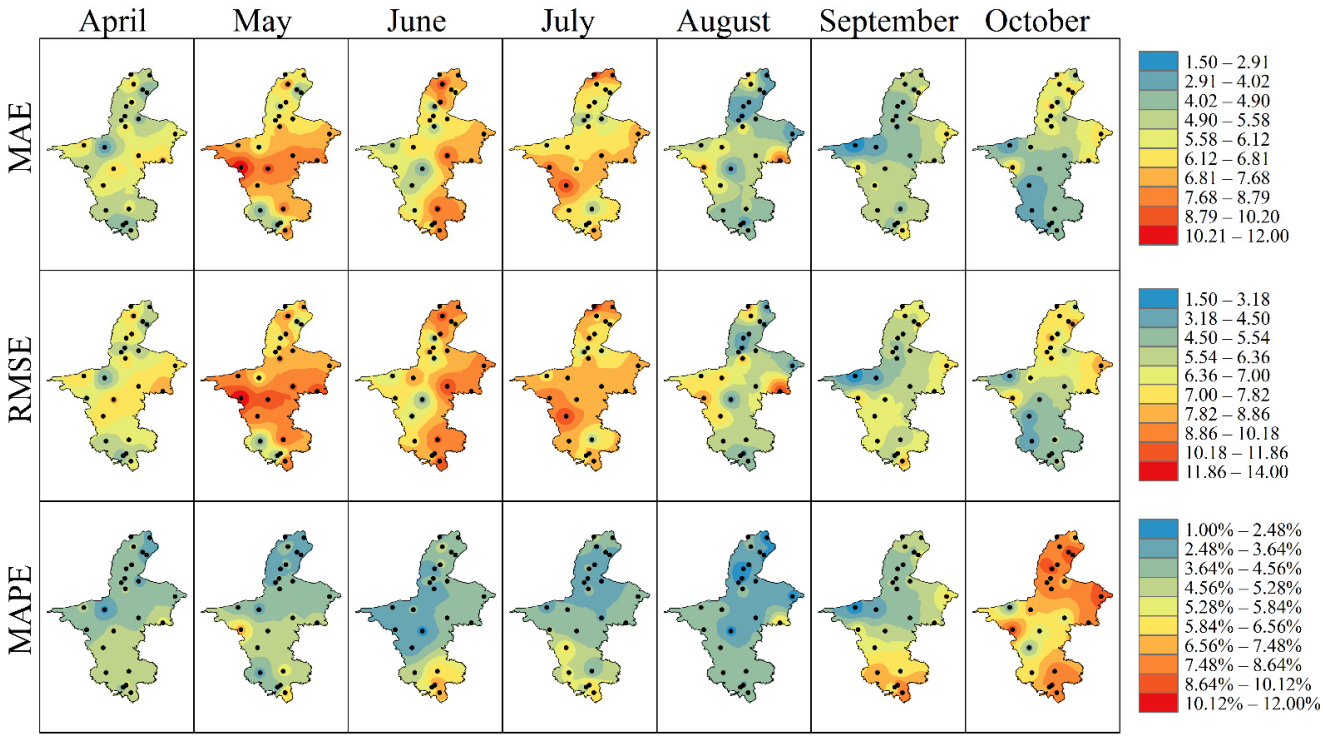

Figure 10. Error analysis of fitted values: mean absolute error (MAE), root mean squared error (RMSE), and mean absolute percentage error (MAPE).

3.2.6. Monthly Extrapolation Forecast of Potential Evaporation in the Growing Season

The monthly forecast and actual values of various regions in Ningxia from 2016 to 2020 are essentially the same, as shown in Figure 11. As shown in Figure 12, the overall range of the mean absolute error (MAE) is between 1.00 and 28.00, and the months with larger red areas are May, June, and July, indicating that the mean absolute error (MAE) is larger. The months with larger blue areas are September and October, indicating that the mean absolute error (MAE) is small. The overall range of the root mean square error (RMSE) is between 1.00 and 35.00, and the distribution is basically consistent with the mean absolute error (MAE). The mean absolute percentage error (MAPE) is mainly between 1.00% and 29.00%. In October, the error is relatively large, with more red areas. Regarding the other months, most are in the yellow area and the blue area (between 1% and 15.16%), with the smallest mean absolute percentage error (MAPE) in August.

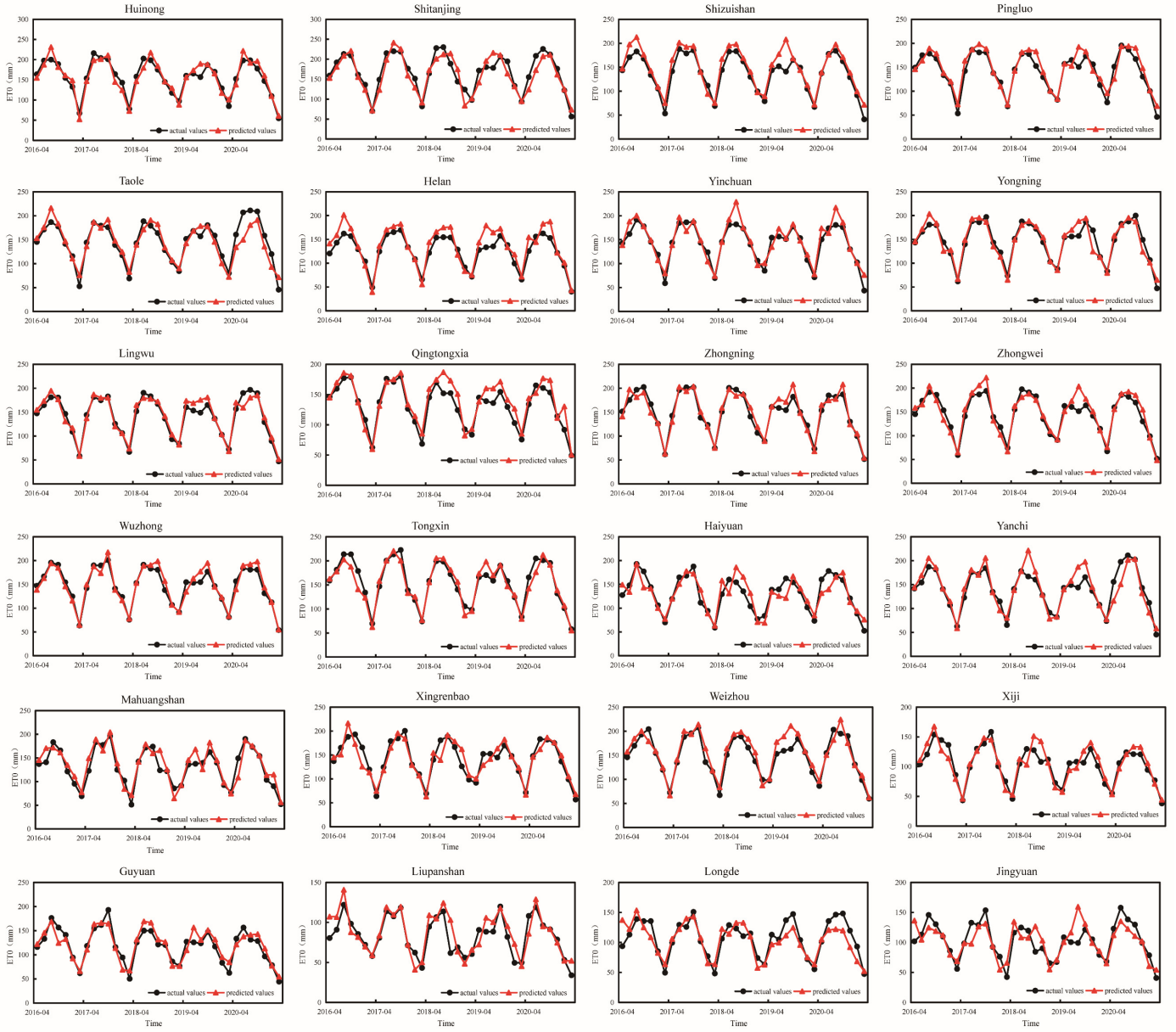

Figure 11. Monthly extrapolated predicted values of potential evaporation in various regions of Ningxia.

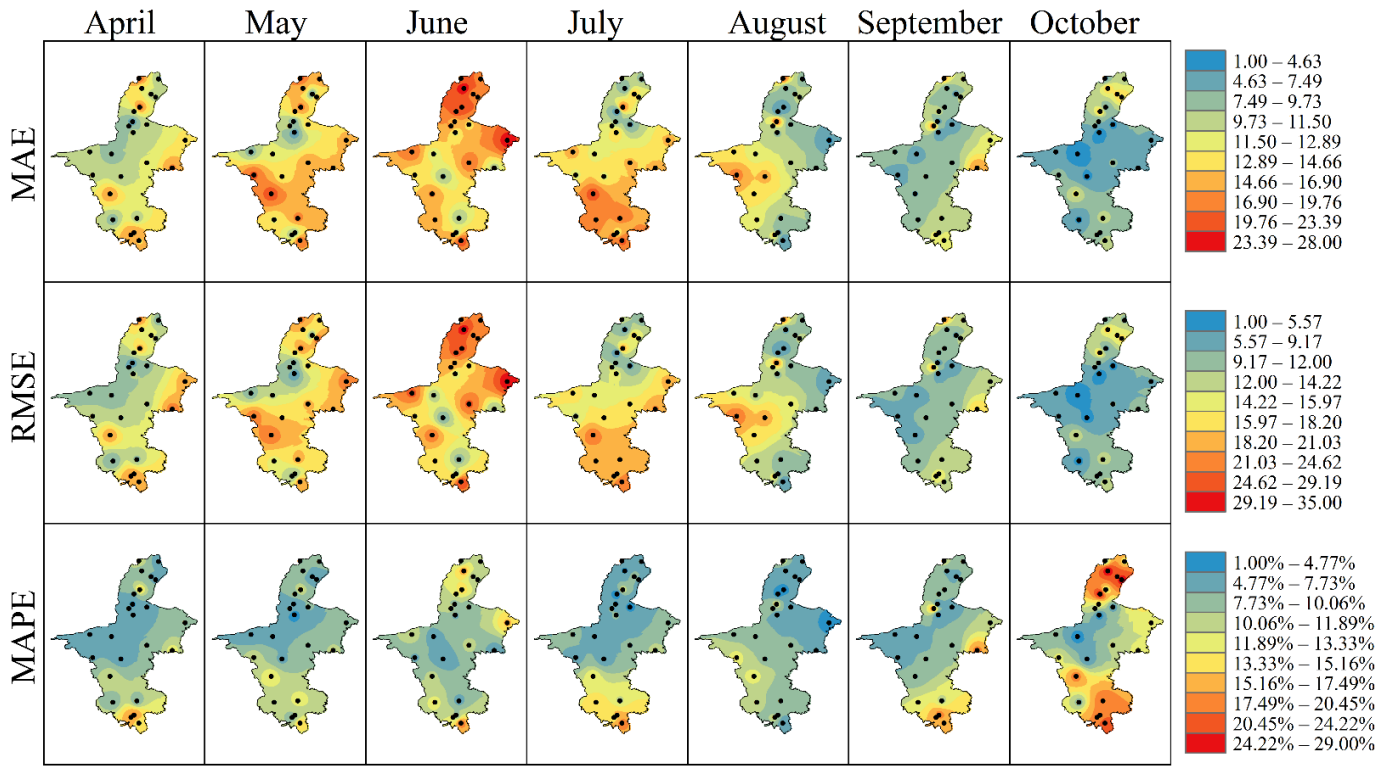

Figure 12. Extrapolated forecast error analysis: mean absolute error (MAE), root mean squared error (RMSE), and mean absolute percentage error (MAPE).

4. Discussion

Evaporation is a bridge in terms of land–atmosphere interactions, and plays an extremely important role in the hydrological cycle and agricultural irrigation [20]. The atmospheric circulation has a strong influence on the potential evaporation in the growing season [21]. Its drastic change has led to the acceleration of the water cycle [22], which has also affected potential evaporation. Previous studies have found that the Arctic Oscillation (AO) is closely related to the mid-to-high latitudes [23], and some studies have shown that the hydrological cycle is important for El Niño Southern Toss. This is closely related to cyclones (NHPV), the Atlantic Oscillation (ENSO), and the North Atlantic Oscillation (NAO) [24], which may affect the change in evaporation through the circulation anomaly, and then affect the occurrence of meteorological and hydrological drought [25]. Other studies have shown that China's climate is mainly affected by the synchronous subtropical high in the western North Pacific and the atmospheric circulation in the mid-to-high latitudes of the North Pacific, as well as the monsoon circulation in the western North Pacific [26,27].

This study describes the temporal and spatial relationship of potential evaporation in the growing season, and uses the step-by-step asymptotic regression method to predict the potential evaporation in the growing season. The results show that the potential evaporation in the growing season from 1990 to 2010 has a larger increasing trend, which is consistent with the fifth IPCC assessment report [28], which provides the conclusion that 1983–2012 was the hottest 30-year period in the past 1400 years. The spatiotemporal analysis of potential evaporation in the growing season shows that the potential evaporation in April, May, and June has shown an increasing trend over the past 30 years. The UF value in July, August, and October was relatively stable, and the potential evaporation was relatively stable. The potential evaporation in September has shown a downward trend over the past 20 years. The prediction results show that the predicted value of the potential evaporation in the growing season is basically consistent with the actual value, the predicted actual value of the potential evaporation in the growing season is basically consistent with the predicted value curve, and the mean absolute percentage error (MAPE) in October is

relatively large. The mean absolute error (MAE) and root mean square error (RMSE) in June were larger.

5. Conclusions

Potential evaporation is an important factor in both the hydrological cycle and farmland irrigation. Based on the daily data of 24 meteorological stations, this paper analyzes the time series changes in potential evaporation during the growing season in Ningxia, and systematically establishes a prediction model of potential evaporation during this period. The hydrological cycle change and farmland irrigation system in Ningxia in the growing season are used to provide a reference. The main conclusions are as follows:

(1) The areas with large potential evaporation in the growing season are mainly the central area and the northern side of the northern area of Ningxia. The western side of the central area of the Ningxia Hui Autonomous Region has a greater increasing trend, and the eastern and northern sides of the Ningxia Hui Autonomous Region have a decreasing trend.

(2) On the monthly scale, the potential evaporation continued to increase from April to June, reached its maximum in June, continued to decrease from July to October, and was the smallest in October. The increasing trend of potential evaporation from April to June and the increasing trend of the west side of the central region are obvious, and the trend of potential evaporation from July to October is more obvious, during which the decreasing trend is most obvious in September, although most areas show a decrease to some extent. Among them, the northern side of the northern region and the eastern side of the central region have the largest decreasing trend.

(3) According to the results of the MK test in the growing season, the change in potential evaporation in the growing season showed a trend of "increase–decrease". According to the results of the monthly scale MK test, the potential evaporation in April, May, and June has shown an increasing trend over the past 30 years. The UF value in August and October has been relatively stable, and the trend of potential evaporation has been relatively stable. The potential evaporation in September has shown a downward trend over the past 20 years.

(4) The prediction model of potential evaporation in the growing season established by atmospheric circulation has shown good results in Ningxia, demonstrating that the circulation factor can be used to establish the scheduling forecast for irrigation water.

Author Contributions: This paper was calculated and written by Z.L., guided by Q.S., and revised and discussed by D.X., W.F., R.W. and P.J. All authors have read and agreed to the published version of the manuscript.

Funding: This study was funded by the National Key Research and Development Program "Research and Demonstration of Key Technologies for the Wine Industry in the Eastern Helan Mountains of Ningxia" (2019YFD1002502).

Institutional Review Board Statement: Not applicable.

Informed Consent Statement: All subjects involved in this study provided informed consent.

Data Availability Statement: Not applicable.

Acknowledgments: Thanks are given to the National Meteorological Center of China Meteorological Administration for providing the meteorological and index datasets.

Conflicts of Interest: The authors declare no conflict of interest.

References

1. Allen, R.G.; Pereira, L.S.; Smith, M.; Raes, D.; Wright, J.L. FAO-56 dual crop coefficient method for estimating evaporation from soil and application extensions. *J. Irrig. Drain. Eng.* **2005**, *131*, 2–13. [CrossRef]
2. Singh, V.P. Volume I: Rainfall-runoff modeling. In *Hydrologic Systems*; Prentice Hall: Englewood Cliffs, NJ, USA, 1988; p. 480.

3. Jaramillo, F.; Prieto, C.; Lyon, S.W.; Destouni, G. Multimethod assessment of evapotranspiration shifts due to non-irrigated agricultural development in Sweden. *J. Hydrol.* **2013**, *484*, 55–62. [CrossRef]
4. Qin, D.; Chen, Z.; Averyt, K.B.; Miller, H.L.; Solomon, S.; Manning, M.; Marquis, M.; Tignor, M. *IPCC, 2007: Summary for Policymakers*; Cambridge University Press: Cambridge, UK, 2007.
5. Waller, P.; Yitayew, M. Crop Evapotranspiration. In *Irrigation and Drainage Engineering*; Springer: Cham, Switzerland, 2016; pp. 89–104.
6. Duce P, Snyder R L, Spano D. Forecasting reference evapotranspiration. In Proceedings of the III International Symposium on Irrigation of Horticultural Crops, Lisbon, Portugal, 1 October 2000.
7. Li, L.; Ni, W.; Li, Y.; Guo, D.; Gao, H. Impacts of Sea Surface Temperature and Atmospheric Teleconnection Patterns in the Northern Mid-Latitudes on Winter Extremely Cold Events in North China. *Adv. Meteorol.* **2021**, *2021*, 853457. [CrossRef]
8. Xu, J.; Li, F. Response of lower Yellow River bank breachings to La Nia events since 924CE. *Catena* **2019**, *176*, 159–169. [CrossRef]
9. Gritsun, A.S. Variability of extra tropical atmospheric circulation and periodic trajectories in simplified models of atmospheric dynamics. *Izv. Atmos. Ocean. Phys.* **2020**, *56*, 229–240. [CrossRef]
10. Kyselý, J. Implications of enhanced persistence of atmospheric circulation for the occurrence and severity of temperature extremes. *Int. J. Climatol. A J. R. Meteorol. Soc.* **2007**, *27*, 689–695. [CrossRef]
11. Schubert, S.; Rienecker, M.; Mlynczak, M.; Miller, T.; Schoeberl, M. Ocean and atmosphere: Predicting monthly to seasonal climate variability and the oceanic and atmospheric causes and effects. In Proceedings of the IGARSS 2003. 2003 IEEE International Geoscience and Remote Sensing Symposium, Toulouse, France, 21–25 July 2003; IEEE: Piscataway, NJ, USA, 2003; Volume 1, pp. 142–144.
12. Jackson, L.C.; Smith, R.S.; Wood, R.A. Ocean and atmosphere feedbacks affecting AMOC hysteresis in a GCM. *Clim. Dyn.* **2017**, *49*, 173–191. [CrossRef]
13. Zheng, J.; Li, B.; Chen, Y.; Chen, Z.; Lian, L. Spatiotemporal variation of upper-air and surface wind speed and its influencing factors in northwestern China during 1980–2012. *Theor. Appl. Climatol.* **2017**, *133*, 1303–1314. [CrossRef]
14. Kononova, N.K.; Lupo, A.R. Changes in the Dynamics of the Northern Hemisphere Atmospheric Circulation and the Relationship to Surface Temperature in the 20th and 21st Centuries. *Atmosphere* **2020**, *11*, 255. [CrossRef]
15. Po-Chedley, S.; Zelinka, M.D.; Jeevanjee, N.; Thorsen, T.J.; Santer, B.D. Climatology explains intermodel spread in tropical upper tropospheric cloud and relative humidity response to greenhouse warming. *Geophys. Res. Lett.* **2019**, *46*, 13399–13409. [CrossRef]
16. Urban, G.; Migała, K.; Pawliczek, P. Sunshine duration and its variability in the main ridge of the Karkonosze Mountains in relation to with atmospheric circulation. *Theor. Appl. Climatol.* **2018**, *131*, 1173–1189. [CrossRef]
17. Ahmadi, S.H.; Fooladmand, H.R. Spatially distributed monthly reference evapotranspiration derived from the calibration of Thornthwaite equation: A case study, South of Iran. *Irrig. Sci.* **2008**, *26*, 303–312. [CrossRef]
18. Heydari, M.M.; Heydari, M. Calibration of Hargreaves–Samani equation for estimating reference evapotranspiration in semiarid and arid regions. *Arch. Agron. Soil Sci.* **2014**, *60*, 695–713. [CrossRef]
19. Heydari, M.M.; Tajamoli, A.; Ghoreishi, S.H.; Darbe-Esfahani, M.K.; Gilasi, H. Erratum to: Evaluation and calibration of Blaney–Criddle equation for estimating reference evapotranspiration in semiarid and arid regions. *Environ. Earth Sci.* **2015**, *74*, 4053–4063. [CrossRef]
20. Xu, Y.P.; Pan, S.; Fu, G.; Tian, Y.; Zhang, X. Future potential evapotranspiration changes and contribution analysis in Zhejiang Province, East China. *J. Geophys. Res. D Atmos. Jgr.* **2014**, *119*, 2174–2192. [CrossRef]
21. Sun, H.; Hu, H.; Wang, Z.; Lai, C. Temporal Variability of Drought in Nine Agricultural Regions of China and the Influence of Atmospheric Circulation. *Atmosphere* **2020**, *11*, 990. [CrossRef]
22. Willems, P. Compound intensity/duration/frequency-relationships of extreme precipitation for two seasons and two storm types. *J. Hydrol.* **2000**, *233*, 189–205. [CrossRef]
23. Hudgins, L. Bivariate wavelet analysis of Asia monsoon and ENSO. *Adv. Atmos. Sci. Engl. Version* **1996**, *13*, 299–312. [CrossRef]
24. Talaee, P.H.; Tabari, H.; Ardakani, S.S. Hydrological drought in the west of Iran and possible association with large-scale atmospheric circulation patterns. *Hydrol. Processes* **2014**, *28*, 764–773. [CrossRef]
25. Huang, S.; Li, P.; Huang, Q.; Leng, G.; Hou, B.; Ma, L. The propagation from meteorological to hydrological drought and its potential influence factors. *J. Hydrol.* **2017**, *547*, 184–195. [CrossRef]
26. Liu, Y. Influence of the Western North Pacific Summer Monsoon on Summer Rainfall over the Yangtze River Basin. *Chin. J. Atmos. Sci.* **2009**, *33*, 1225–1237.
27. Zhang, Q.Y.; Tao, S.Y. Tropical and subtropical monsoon over east asia and its influence on the rainfall over eastern china in summer. *Q. J. Appl. Meteorl.* **1998**, *9*, 17–23.
28. *Climate Change 2013: The Physical Science Basis*; Working Group I Contribution to the Fifth Assessment Report of the Intergovernmental Panel on Climate Change; Cambridge University Press: New York, NY, USA, 2013; Available online: https://www.ipcc.ch/site/assets/uploads/2017/09/WG1AR5_Frontmatter_FINAL.pdf (accessed on 10 August 2022).